*

Surface Functionalization and Humidity on Charge Transport in PP/TiO_2 and PP/MgO Nanocomposites

Phichet Ketsamee, Alun Vaughan, and Thomas Andritsch

***Abstract*— This study investigates the influence of polar silane coupling agents on charge transport in polypropylene (PP) nanocomposites containing magnesium oxide (MgO) and titanium dioxide (TiO_2) nanoparticles in the presence of water molecules. Surface functionalization results in reduced charge accumulation and electrical conductivity compared to unmodified nanocomposites. Under vacuum-dried conditions, the charge transport is primarily dominated by the types of nanoparticles. It is hypothesized that band bending at the interfaces of MgO used in the PP matrix is more effective in suppressing charges than TiO_2. Regarding humidity, the extent of water absorption not only influences charge transport but also contributes to the bonding states between water molecules and nanoparticle surfaces. Despite higher water absorption, band bending at the interfaces in PP/MgO potentially limits the increase in charge transport. Additionally, differences in electronegativity during surface functionalization would lead to distinct bonding states with water molecules, resulting in varying energy band levels at interfaces, which in turn influence the ability of materials to capture charge carriers. The most effective charge suppression and reduced electrical conductivity are achieved in ethoxy-modified materials with amino functional groups.**

***Index Terms*—band bending, charge transport, electronegativity, humidity, magnesium oxide, polypropylene, surface functionalization, titanium dioxide**

I. INTRODUCTION

POLYPROPYLENE (PP) is a promising alternative to cross-linked polyethylene (XLPE) for high voltage (HV) cable insulation materials. The high operating temperature of PP potentially eliminates the need for crosslinking agents and, therefore, the requirement for lengthy degassing procedures [1]. As a thermoplastic material, PP is more easily recyclable, thus significantly reducing environmental impact at the end of its service life compared to XLPE.

Unmodified PP, however, has specific drawbacks and cannot be readily used as insulation for HV cables. PP exhibits high brittleness at room temperature, attributed to its high glass transition temperature [2]. With a lower thermal conductivity of PP (0.11-0.22 W/m K) compared to 0.32 W/m·K for commercial XLPE [3], the increased thermal headroom due to the higher melting point of PP is rather restricted. Additionally, PP tends to form particularly large spherulites. The electrical breakdown process of PP typically occurs through the inter-spherulitic regions, creating electrically weak pathways within the structure.

The tuning of dielectric properties in polymers can be achieved by incorporating nanosized fillers. The dispersion of nanoparticles is closely related to determining the dielectric properties of the nanocomposites [4]. However, nanoparticles typically tend to agglomerate; therefore, surface functionalization is employed to enhance their dispersion and improve dielectric properties [5].

In addition to the dispersion of nanoparticles, the dielectric properties of PP nanocomposites also vary depending on the type of surface functionalization. The use of different polar silane coupling agents (SCA) on nanoparticle surfaces, containing polar groups or heteroatoms (i.e., S, O, or N) with different electronegativities compared to hydrocarbons in PP, demonstrated the introduction of deeper traps compared to non-polar agents [6]. This, in turn, had a positive impact on a variety of bulk properties.

Titanium dioxide (TiO_2) and magnesium oxide (MgO) are good options, as both particles have been shown to improve the dielectric properties of PP nanocomposites. The key findings regarding the enhanced dielectric properties of PP/TiO_2- and PP/MgO-based materials from elsewhere were summarized in our previous work [7]. Additionally, we demonstrated that incorporating TiO_2 and MgO nanoparticles into PP, treated with various polar SCA, resulted in a decrease in dielectric losses under vacuum-dried conditions [8]. Interestingly, under humid conditions [7], composites with 5 weight percentage (wt.%) of TiO_2 and MgO SCA-modified nanoparticles exhibited a different polarizability based on the state of the bonding water and polar functionalization. In other words, the different measured relaxation peaks were related to the SCA on the surfaces, rather than the bulk of the nanoparticles.

Kubyshkina *et al.* [9][10] presented a charge dynamics model for nanocomposites based on density functional theory (DFT). The authors proposed that using nanoparticles with

*This paragraph of the first footnote will contain the date on which you submitted your paper for review, which is populated by IEEE. *(Corresponding author: Phichet Ketsamee).*

Phichet Ketsamee, Alun Vaughan, and Thomas Andritsch are with The Tony Davies High Voltage Laboratory, School of Electronics and Computer Science, University of Southampton, Southampton, SO17 1BJ, United Kingdom, (e-mail: pk1r18@soton.ac.uk).

different electronic properties, most importantly different band gaps and electron affinity, leads to two different mechanisms of band alignment at the interfaces. If the nanoparticle possesses positive electron affinity and has a significantly narrower band gap than the polymer matrix, then the whole particle will have the lowest energy states and act as a charge carrier trap. Alternatively, if both the nanoparticle and polymer matrix exhibit negative electron affinity and have comparable band gaps, then so-called band bending will take place at the interface between the polymer and the nanoparticle, resulting in the localization of the lowest energy states.

This work focuses on analyzing the effects of TiO_2 and MgO nanoparticles, which possess different band gaps, in a PP matrix, thereby producing experimental results to test the above hypothesis. The nanoparticles were modified using three different polar SCA, and the composites were tested under different environmental conditions. The main objective is to investigate the influence of nanoparticle surface functionalization and water absorption on space charge dynamics and DC conductivity. The dispersion of the nanofillers within the composites was examined using scanning electron microscopy (SEM). The crystal structure and thermal properties of the composites were assessed through X-ray diffraction (XRD) and differential scanning calorimetry (DSC).

II. Materials And Sample Preparations

A. Materials

Isotactic PP (427861) was obtained from Sigma Aldrich. TiO_2 (7910DL) and MgO (4800DL) nanoparticles, both with a spherical shape and a mean particle size of 10-30 nm, as specified by the manufacturer, were purchased from SkySpring Nanomaterial, Inc. Polar SCA with different hydrolyzable and organofunctional groups were obtained from the following suppliers: 3-trimethoxysilyl propyl methacrylate (MM) was purchased from Sigma Aldrich; both 3-aminopropyl trimethoxy (MA) and 3-aminopropyl triethoxy (EA) silanes were obtained from Aladdin industrial Inc.

B. Surface Functionalization of Nanoparticles

An anhydrous method was used to prepare surface-modified TiO_2 and MgO nanofillers with three different polar SCA consisting of MM, MA, and EA. Nano powder was added to 0.1 g/mL of dry toluene, and the nanofiller/dry toluene mixture was sonicated for 1 h. The mixture was poured into an evaporation flask, and then 0.2 mL of SCA was slowly added. This quantity was determined to prevent the saturation reaction point [11]. The resulting mixture underwent stirring using a magnetic stirrer on a hotplate and was heated to reflux at the boiling point of toluene for 4 h. The obtained slurry was washed three times with 100 mL of fresh toluene and centrifuged at 8000 rpm to remove any excess SCA. Finally, the solvent was evaporated for 48 h in a fume cupboard before being placed in a vacuum oven for an additional 24 h to remove the remaining solvent.

The anhydrous method involves no hydrolysis to mitigate the condensation of SCA; instead, substitution mechanisms are described for the bonding reaction between nanoparticle surfaces and SCA [12]. Thermogravimetric analysis (TGA) successfully confirmed the presence of grafted SCA in both TiO_2 and MgO [8], indicating that the rate of grafting depends on the hydrolyzable groups. Methoxy group of MM and MA reacted faster with both nanoparticle surfaces compared to the ethoxy group of EA.

C. Preparations of Polymer Nanocomposite

PP nanocomposites with varying contents of TiO_2 and MgO nanofillers (0.5, 2.5, and 5 wt.%) were prepared using a solution blending method. The desired amount of nano powder, both untreated and treated, was dispersed in 10 mL of xylene and sonicated with a probe sonicator for 30 min to break the agglomerations. To prevent overheating caused by using high sonication power, the nanofiller/xylene sample tube was immersed in water during sonication. Simultaneously, PP pellets were dissolved in 50 mL of xylene using a magnetic stirrer with a hotplate set to 200 °C. The nanofiller/xylene solvent was then poured into a PP/xylene solvent and stirred continuously for 1 min before being poured into 90 mL of methanol. The precipitated solid was filtered using a Büchner funnel and dried for 24 h in a fume cupboard, followed by additional drying in a vacuum oven at 80 °C for 72 h. Dry solid material was pressed at 180 °C and then further processed into thin films with desired shapes and thickness, according to each experimental requirement, using a hydraulic press. Then, the thin film was quenched directly in distilled water at room temperature (~20 °C). Finally, the thickness of all the samples was measured at multiple points to confirm the average thickness.

The prepared thin films underwent two different environmental conditions: 1) vacuum-dried samples were placed in a vacuum oven at 80 ºC for 72 h before being stored in a vacuum desiccator, and 2) humid samples were immersed in deionized water for 21 d. The humid samples were periodically weighed using a microbalance with a precision of 0.1 mg until the weight became stable. The change in mass of PP nanocomposites, measured at room temperature after 21 d of immersion in water, was discussed in previous work [7].

PP/nanofiller/SCA/filler content/environmental condition was used to identify samples. For example, PP/TiO_2/EA/5/H indicates that PP was combined with 5 wt.% of TiO_2 that had been coated with 3-aminopropyl triethoxy and immersed in water (H); while D stands for vacuum-dried samples.

III. Characterization

Samples for examination by SEM were prepared using the permanganic etching technique described in [7]. After being coated with gold using an Emitech K550X sputter coater, the samples were examined at a 20 kV accelerating voltage with a Zeiss EVO50XVP.

The melting and crystallization behavior of the materials was examined using a Mettler Toledo DSC-820 Differential Scanning Calorimeter. Each sample, weighing ~5 mg, was placed in an aluminum container and heated from 20 °C to

200 °C, held for 5 min and then cooled from 200 °C to 20 °C. Heating and cooling were performed at 10 °C/min in nitrogen.

XRD was used to investigate the crystalline structure, using a Bruker Power X-ray Diffraction, D2 Phaser. Diffraction patterns were recorded from 2θ = 10° to 80° with λ = 1.54184 Å and a step size of 0.0202° using film samples, 200±10 µm in thickness.

A pulsed electro-acoustic (PEA) system was used to investigate space charge behavior, according to IEC/TS 62758. In this, a voltage pulse (amplitude 600 V and pulse width 5 ns) was used to induce an acoustic signal in the sample of thickness 200±10 µm. Data were collected at room temperature for an hour under an applied electric field of +40 kV/mm (poling), followed immediately with the short-circuit process for another hour (de-poling). The resulting data were analyzed using LabVIEW.

DC conductivity measurements were carried out according to ASTM D257-14. Samples 100±10 µm in thickness were sandwiched between two electrodes with a guard ring 30 mm in diameter. The conduction current was measured every 1 s over a period of 3600 s, using a Keithley 486 picometer. Data were collected at room temperature with the same applied field of +40 kV/mm using LabVIEW.

IV. Results

A. Scanning Electron Microscopy

SEM images of 5 wt.% PP/TiO_2 and PP/MgO samples were presented in [7]. The results showed a similar trend among amino-based materials, while MM-modified samples exhibited agglomeration that is on average approximately 1-2 µm larger. Here we focus on untreated and EA-treated samples with 2.5 and 5 wt.%, as depicted in Fig. 1. In samples with higher filler contents, larger particle agglomerations can be seen. In both untreated PP/TiO_2 and PP/MgO samples, the agglomeration size in the 5 wt.% samples are around 5 µm, which is larger than the 1-2 µm observed in the untreated 2.5 wt.% samples. Functionalization significantly reduces the agglomerate size, by approximately 50% in the 5 wt.% samples, although this effect is difficult to confirm for the samples loaded to 2.5 wt.%.

B. Thermal and Crystal Evaluation

Previous findings [7] have suggested that the DSC melting (T_m) and crystallization (T_c) behavior of PP containing 5 wt.% of TiO_2 and MgO nanoparticles remains similar, regardless of functionalization. This study confirms that the T_m of these samples is comparable to unfilled PP, remaining at 161 °C, and that this value is unaffected by varying the nanofiller contents. Fig. 2 displays the T_c of untreated and EA-treated PP nanocomposites with different filler loadings. As the nanofiller content increases, T_c shows a consistent increase, reaching 7-8 °C higher in the samples containing 5 wt.% of nanofiller.

TGA measurements of the weight loss of TiO_2 and MgO nanoparticles, demonstrates that untreated MgO had a higher weight loss compared to untreated TiO_2 [7][8]. It appears that untreated MgO has more surface functional groups, and in all cases, treated MgO exhibits a greater mass loss than TiO_2 when considering the same SCA. This suggests significant differences in the surface structure between TiO_2 and MgO. The presence of different amounts and surface structures of MgO and TiO_2 nanoparticles in the PP matrix would result in a different rate of crystallization, influenced by the number of nuclei and the subsequent crystal growth rate in the systems.

XRD curves acquired from EA-treated PP/TiO_2 and PP/MgO samples containing 0.5 and 5 wt.% of filler are presented in Fig. 3. The XRD diffractogram of both neat PP and PP nanocomposites exhibits distinct peaks at 2θ = 14.1°, 17°, 18.6°, 21.3°, 21.8°, 25.6°, and 28.7°, which correspond to the (110), (040), (130), (111), (131)/(041), (060), and (220) crystal planes of the PP α-crystal (monoclinic) structure [13].

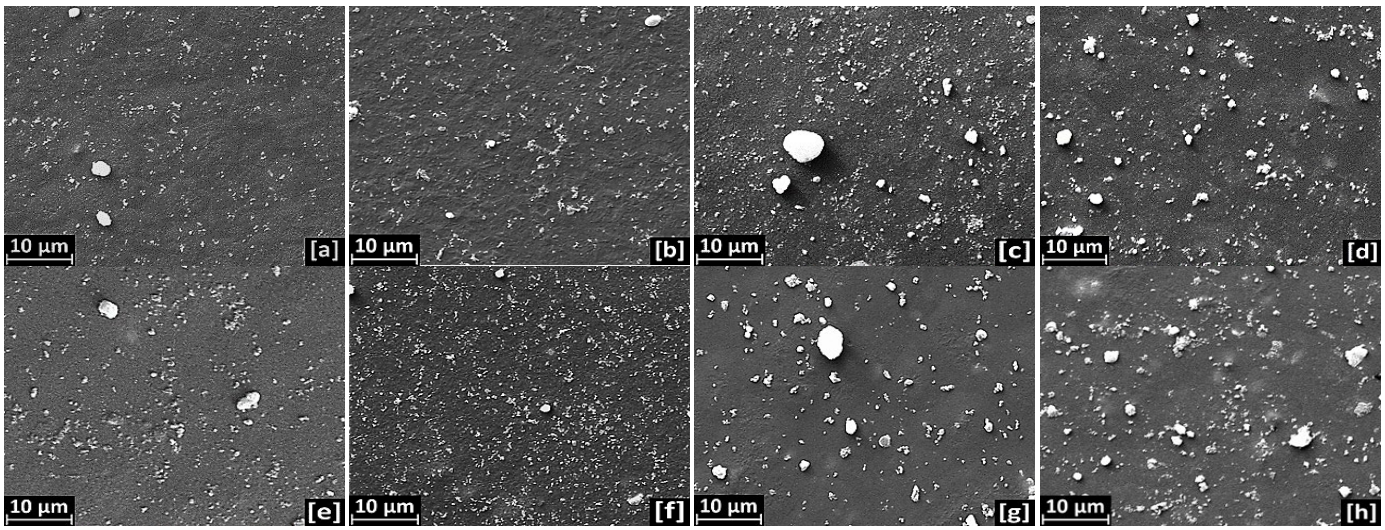

Fig. 1. SEM images of (a) PP/TiO_2/2.5/D, (b) PP/TiO_2/EA/2.5/D, (c) PP/TiO_2/5/D, (d) PP/TiO_2/EA/5/D, (e) PP/MgO/2.5/D, (f) PP/MgO/EA/2.5/D, (g) PP/MgO/5/D, and (h) PP/MgO/EA/5/D samples.

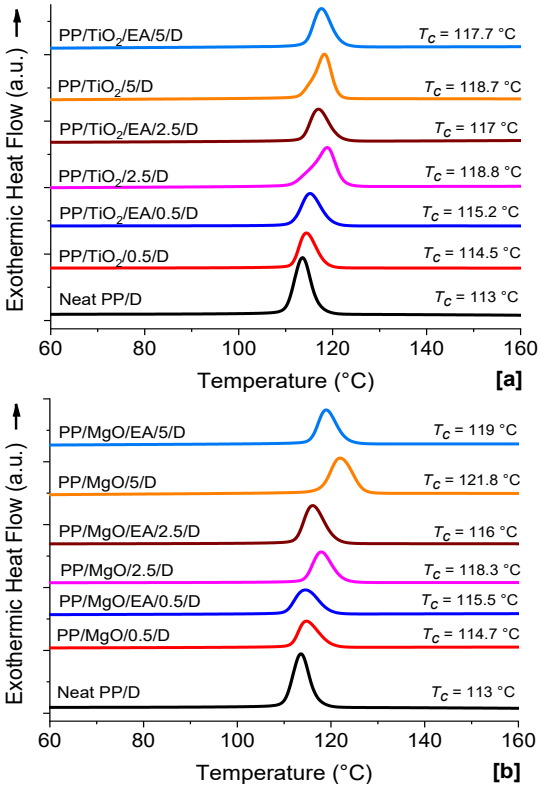

Fig. 2. DSC crystallization temperatures of different filler contents in (a) PP/TiO_2 and (b) PP/MgO samples.

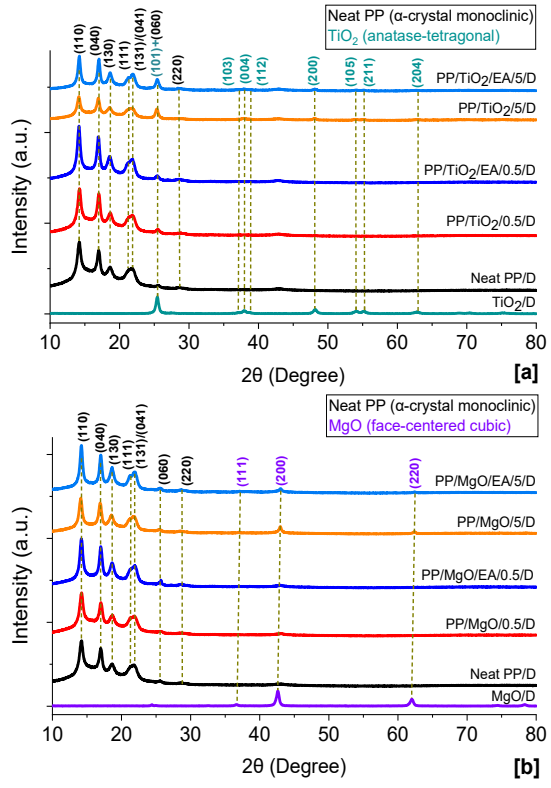

Fig. 3. XRD diffractogram of different filler contents in (a) PP/TiO_2 and (b) PP/MgO samples.

The presence of anatase (tetragonal) TiO_2 is indicated by the strong diffraction peaks observed at 25° (101) and 48° (200) [14]. Additionally, the peaks at 36.9° (111), 42.9° (200), and 62.3° (220) indicate the presence of face-centered cubic (FCC) structured MgO nanoparticles [15].

The crystallinity of 5 wt.% PP/TiO_2 and PP/MgO systems, as measured by DSC, exhibited no significant change with different functionalization types, as previously reported [7]. Table I compares the overall crystallinity values obtained by DSC and XRD in untreated and EA-treated samples with different filler contents. The XRD crystallinity (χ_{XRD}) was calculated using OriginLab, by dividing the total area of the crystalline peaks by the corresponding area of all peaks, while the details of the DSC crystallinity (χ_{DSC}) calculation were described in [16]. Neat PP has 55.3±3.4% crystallinity, as determined by XRD, which is similar to the 52.8±2.5% crystallinity obtained from DSC. Both techniques show a similar trend in χ_{XRD} and χ_{DSC} values; the presence of nanoparticles in the 0.5 wt.% samples result in an approximately 8% higher level of crystallinity compared to neat PP, as observed in both measurements. This suggests that the incorporation of TiO_2 and MgO nanoparticles into a PP matrix influences the material morphology, affecting both nucleation density and overall crystallinity. However, in 5 wt.% samples, which exhibited a higher nucleation density and faster crystallization rate (Fig. 2), the crystallinity decreases by more than 5% compared to the 0.5 wt.% samples. This decreases in crystallinity can be attributed to agglomeration, which leads to the formation of molecular chain blocks [17]. Initially, the nanofillers act as nuclei for heterogeneous crystallization, but as the filler content increases, the mobility of the polymer chains becomes restricted, resulting in a constrained network and reduced crystal growth [17].

C. DC Conductivity

Fig. 4 shows the steady-state DC conductivity of both untreated and EA-treated PP/TiO_2 and PP/MgO samples with varying filler contents under vacuum-dried conditions. Due to a similar trend among differently functionalized samples, MM- and MA-treated samples were omitted for brevity.

TABLE I
CRYSTALLINITY OF DIFFERENT FILLER CONTENTS IN PP/TiO_2 AND PP/MgO NANOCOMPOSITES FROM XRD AND DSC.

Nanocomposites	Crystallinity (%)		Nanocomposites	Crystallinity (%)	
	χ_{DSC}	χ_{XRD}		χ_{DSC}	χ_{XRD}
Neat PP/D	52.8±2.5	55.3±3.4			
PP/TiO_2/0.5/D	57.8±1.8	60.9±2.9	PP/MgO/0.5/D	56.8±2.1	60.5±1.6
PP/TiO_2/EA/0.5/D	60.6±1.9	63.5±3.1	PP/MgO/EA/0.5/D	59.5±1.3	63.3±1.2
PP/TiO_2/2.5/D	56.2±2	58.4±2.6	PP/MgO/2.5/D	56.1±1.1	58.9±2
PP/TiO_2/EA/2.5/D	57.6±0.9	60±2.4	PP/MgO/EA/2.5/D	57.7±1.2	60.5±2.4
PP/TiO_2/5/D	53.6±1.2	56.7±3	PP/MgO/5/D	55.1±0.4	57.4±1.3
PP/TiO_2/EA/5/D	55.3±1.1	57.9±3.1	PP/MgO/EA/5/D	55.7±1.5	59.4±2

Each conductivity value was determined by calculating the average of the last ten data points, which were collected from 3591 to 3600 s. For unmodified PP samples, the derived conductivity reaches a steady-state value around 2×10^{-16} S/cm, consistent with the results reported in [18].

The conductivity of PP/TiO_2 and PP/MgO samples (Fig. 4) increases progressively with increased filler content. There are no significant differences in electrical conductivity between treated and untreated samples at filler contents less than 5 wt.%. The lowest conductivity is observed at 0.5 wt.% of nanofiller; it is an order of magnitude lower than that of neat PP and approaches the equipment sensitivity limit (~4×10^{-17} S/cm). These findings are in line with results reported in [19][20], which indicate that the conductivity of low-density polyethylene/MgO and polyimide/TiO_2 composites with filler contents below 3 wt.% was lower than that of the corresponding unfilled polymer. The authors claimed that at low filler content, the reduction in electrical conductivity compared to unfilled polymers is attributed to the effective dispersion of nanofillers. This, in turn, results in a larger separation between nanoparticles, thereby inhibiting the movement of charge carriers trapped at the interface or surface of the nanofillers.

Due to the similar trends among differently functionalized samples in both PP/TiO_2 and PP/MgO, only vacuum-dried 5 wt.% samples were compared with humid samples. The calculated steady-state DC conductivity, as shown in Fig. 5, indicates that there are no significant differences in conductivity between vacuum-dried PP and humid PP. This lack of difference can be attributed to the low water uptake (<0.05%) [7]. In contrast, the steady-state conductivity values obtained from humid PP/TiO_2 and PP/MgO samples are significantly higher than those obtained from equivalent vacuum-dried systems. In general, the conductivity increased from 10^{-15} S/cm in the vacuum-dried samples to 10^{-14} S/cm in the humid samples.

The increase in DC conductivity compared to the vacuum-dried analogues is more pronounced in PP/TiO_2 than in PP/MgO systems. For example, untreated PP/TiO_2 has an increased conductivity around 6.9×10^{-15} S/cm, as opposed to 2.4×10^{-15} S/cm for untreated PP/MgO. EA-treated PP/TiO_2 increased by 2.9×10^{-15} S/cm, while in PP/MgO, with the same functionalization, it increased by 1.4×10^{-15} S/cm.

Fig. 5 demonstrates that DC conductivity values differed more in humid PP/MgO than in PP/TiO_2 samples. The water content in the nanocomposites would drop with time as the experiment was carried out under ambient conditions. After 1 h of experiment, the sample mass, representing water lost during testing, showed that the humid untreated PP/MgO experienced approximately 0.21 mg more mass loss than the humid untreated PP/TiO_2. This is similar to the findings in [21], which showed that after testing DC conductivity, the mass of the samples decreased due to a decrease in the water content in nanocomposites composed of polyethylene (PE) and boron nitride.

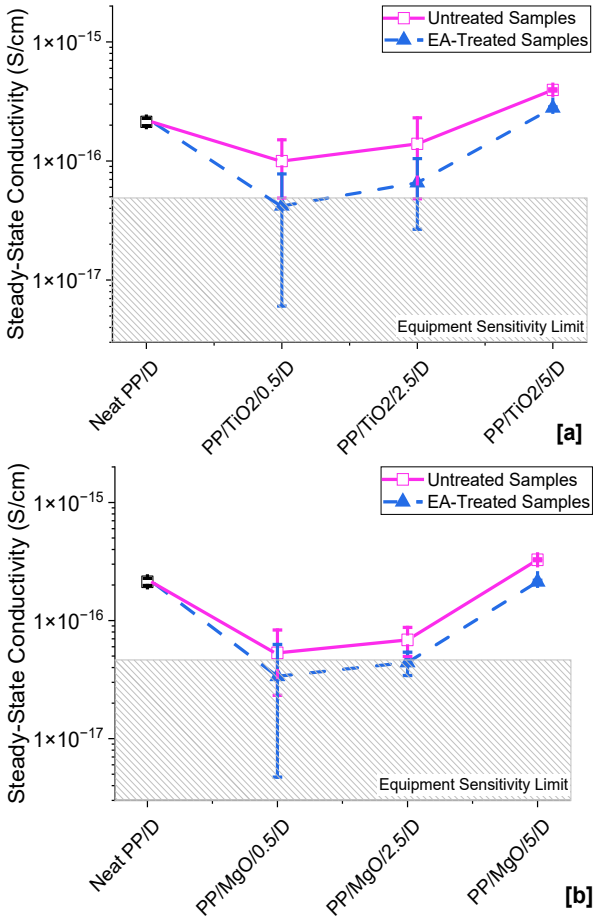

Fig. 4. Steady-state DC conductivity with untreated and EA-treated (a) PP/TiO_2 and (b) PP/MgO with different filler contents under vacuum-dried conditions.

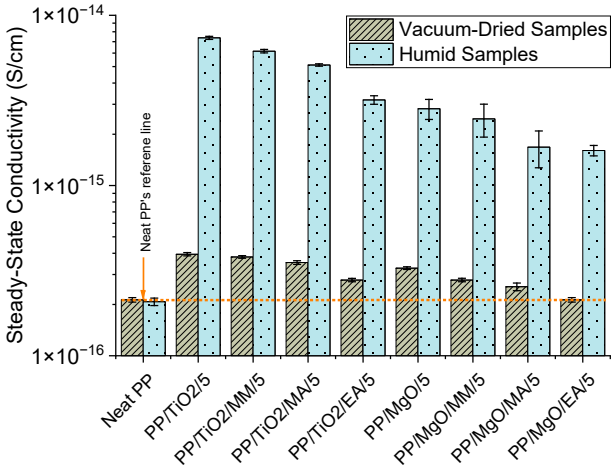

Fig. 5. Comparison of the steady-state DC conductivity under vacuum-dried and humid conditions.

D. Space Charge Dynamics

Since PEA measures the net accumulated charge within the complete system, we first used a subtraction method, as expressed in (1) by Liu *et al.* [22], to estimate the charge density in the bulk of each sample. This method mitigates the influence of capacitive charges on the electrodes and provides a more detailed reflection of the charge distribution in the bulk.

$$\rho_{acc}(x) = \rho_{app}(x) - \frac{V_{app}}{V_{ref}} \cdot \rho_{ref}(x) \quad (1)$$

where $\rho_{acc}(x)$ is charge density after subtraction, $\rho_{app}(x)$ and $\rho_{ref}(x)$ are the charge densities at the applied voltage and reference voltage, respectively, and V_{ref} and V_{app} are the reference and applied voltages.

Subsequently, the net accumulated charge (Q) and the number of charges per unit volume (n) within the bulk of materials were calculated using (2) and (3), respectively. Here, $\rho(x)$ represents the charge density, d is the thickness of the samples (200 µm), S is the area of the electrode (50.26 mm^2), and q is the unit charge of 1.60218×10^{-19} C.

$$Q = \int_0^d |\rho(x)|\, S\, dx \quad (2)$$

$$n = \frac{Q}{(S \cdot d \cdot q)} \quad (3)$$

Fig. 6 shows the total charge accumulation in both untreated and EA-treated systems of PP/TiO_2 and PP/MgO after 1 h of poling. MM- and MA-treated samples were omitted for brevity due to their negligible differences compared to EA samples. The lowest charge accumulation is obtained when both nanofillers are present at 0.5 wt.%; further increases in filler content result in a proportional increase in charge accumulation. At the highest weight percentage, the quantity of charge buildup in PP/MgO systems was less than neat PP, while the charge buildup in PP/TiO_2, especially untreated samples, was significantly higher. Under vacuum-dried conditions, the polar SCA-grafted samples exhibited significantly lower charge accumulation compared to the untreated samples, particularly for 5 wt.% samples. However, for both nanofillers, changing the SCA led to no significant difference in space charge dynamics.

To further investigate the effects of surface functionalization, samples containing 5 wt.% PP/TiO_2 and PP/MgO were immersed in water. Fig. 7 compares the calculated the total charge accumulation after 1 h of poling of 5 wt.% PP/TiO_2 and PP/MgO in vacuum-dried and humid conditions. Neat PP exhibits no significant change, due to low water absorption [7]. In contrast, both untreated and treated nanocomposites show significantly increased charge accumulation after exposure to water. Compared to the vacuum-dried samples, the integrated charge increases by about 3.6×10^{-8} C in untreated PP/TiO_2, which is greater than the 2.8×10^{-8} C increase seen in the equivalent system containing untreated MgO. Similarly, for treated samples, considered the same surface functionalization, PP/TiO_2 have higher charge increases than PP/MgO; for instance, EA-TiO_2 has charge increase of 6.9×10^{-9} C, higher than 5.8×10^{-9} C of EA-MgO.

Space charge profiles of vacuum-dried unfilled PP and 5 wt.% untreated and EA-treated samples are depicted in Fig. 8 and Fig. 9 (a) to (d). Neat PP shows a gradual homocharge injection from the cathode, where negative charges exhibit higher mobility than positive charges [23]. In the case of nanocomposites, charge injection is clearly observed from both electrodes in the untreated PP/TiO_2 samples (Fig. 9 (a)). These charges migrate further into the middle of the bulk with increasing poling time. Treated PP/TiO_2 exhibits a reduction in homocharge compared to untreated PP/TiO_2, as depicted in Fig. 9 (b). In contrast, the space charge profile results in

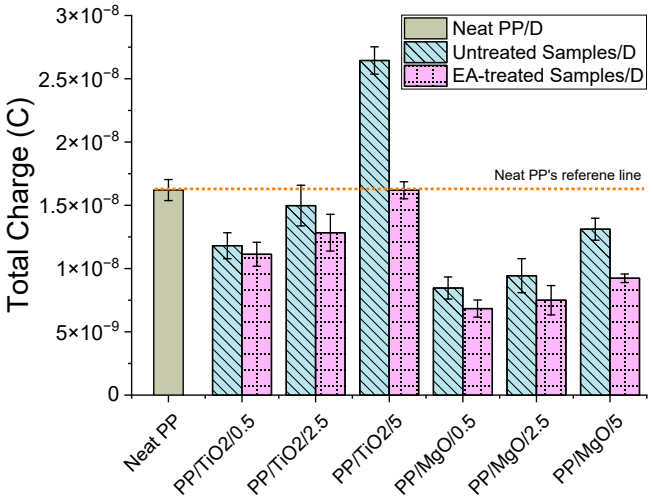

Fig. 6. The total charge of untreated and EA-treated PP nanocomposites with different filler contents under +40 kV/mm in vacuum-dried conditions.

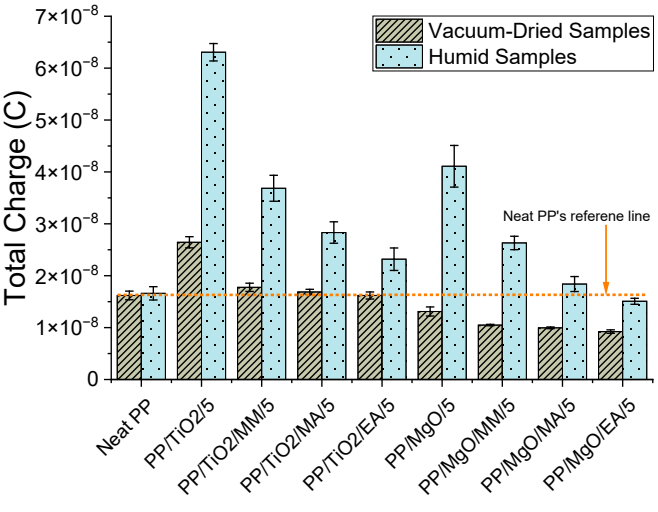

Fig. 7. Comparison of the total charge accumulation after 1 h of poling in vacuum-dried and humid conditions.

Fig. 9 (c) and (d) demonstrate that no apparent charge injection into the MgO bulk is observed, especially in treated PP/MgO. These findings align with the results presented in Fig. 6, which indicate that 5 wt.% PP/MgO exhibits lower charge accumulation compared to neat PP and PP/TiO_2 under equivalent surface conditions. Due to the similarities in agglomeration, crystallinity, and crystal structures observed in the vacuum-dried samples shown in Fig. 1 to Fig. 3, this suggests that changes in microstructure at this high filler content are not directly linked to the space charge dynamics. It appears that the untreated samples exhibit varying degrees of charge accumulation depending on the nanoparticle used. MgO nanoparticles are more effective at suppressing space charge injection in PP than TiO_2.

The presence of water molecules facilitates increased charge injection in all PP/TiO_2 and PP/MgO samples, as shown in Fig. 9 (e) to (h). These charges migrate towards the center of the bulk immediately after the application of a DC voltage. Typically, water dissociates into hydronium (H_3O^+) and hydroxyl (OH^-) ions, which will subsequently migrate under the action of an applied field. The results reported in [24] suggested that such ions move towards the opposite polarity electrodes to form heterocharge, and this heterocharge increases with poling time. The authors stated that the accumulation of heterocharge results in an increased electric field strength near the electrodes, which reduces the charge injection barrier and leads to the accumulation of homocharges within the bulk of the material. The experimental findings, as reported in [24], contrast with the results presented in this work, which demonstrate a dominance of homocharge accumulation. Heterocharge is hardly observable, except in untreated samples (see Fig. 9 (e) and (g)).

To investigate the effect of water absorption on charge accumulation behavior, we estimated the total number of charges per unit volume in the bulk of samples using (3); approximately 3.9×10^{19} m^{-3} for untreated PP/TiO_2/5 and 2.5×10^{19} m^{-3} for untreated PP/MgO/5. The extent of water ionization can be calculated for any system containing a known amount of water. The quantities of each H_3O^+ and OH^- ion component per unit volume, calculated from the water amount, reported in [7], are 7.6×10^{9} m^{-3} for untreated PP/TiO_2/5 and 2.1×10^{10} m^{-3} for untreated PP/MgO/5. The calculated value of water ionization is significantly lower compared to the total number of charges in the bulk. This suggest that the amount of injected homocharge is significantly higher than the number of water-derived ions. This, in turn, may lead to a reduction in the

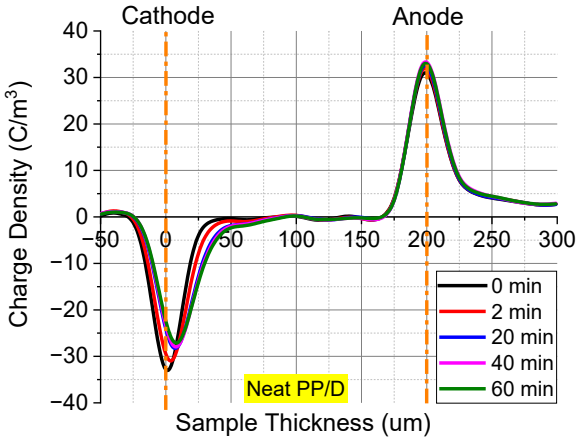

Fig. 8. Space charge profiles of unfilled PP under vacuum-dried condition.

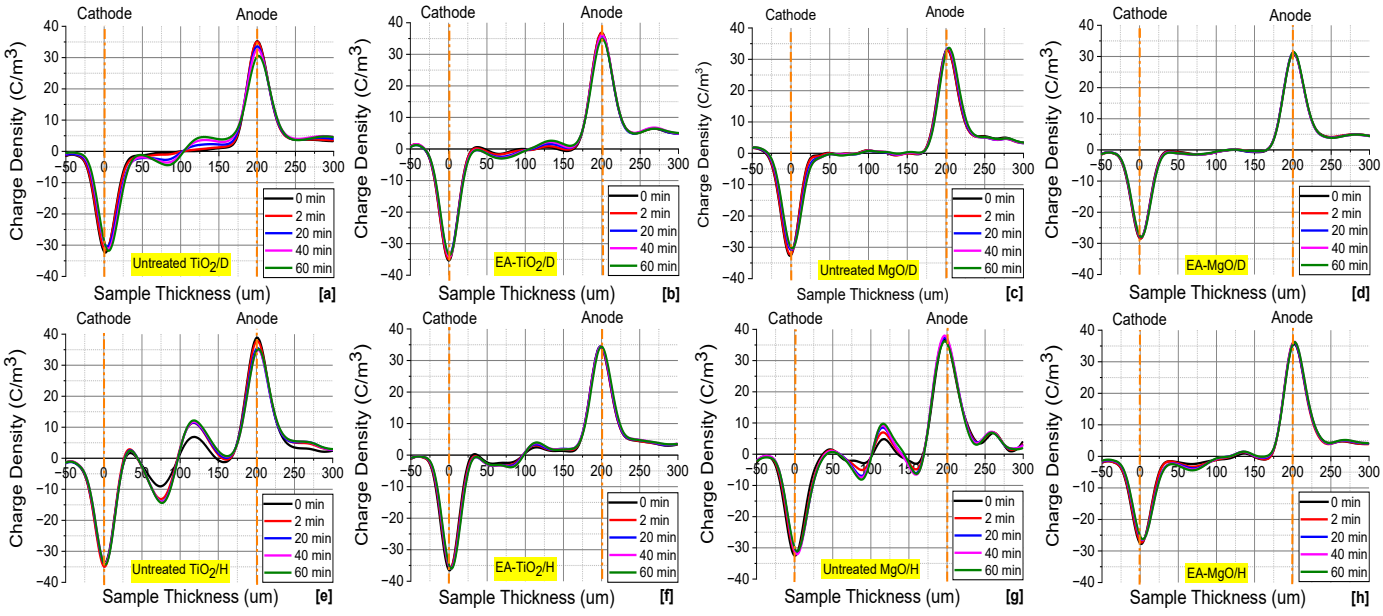

Fig. 9. Space charge profiles with different SCA under vacuum-dried conditions of (a) PP/TiO_2/5/D, (b) PP/TiO_2/EA/5/D, (c) PP/MgO/5/D, and (d) PP/MgO/EA/5/D samples, as well as under humid conditions of (e) PP/TiO_2/5/H, (f) PP/TiO_2/EA/5/H, (g) PP/MgO/5/H, and (h) PP/MgO/EA/5/H samples.

measured charge density of heterocharge from water ionization, as the PEA technique can only measure net charges in the samples.

Regarding the effects of surface functionalization in humid conditions, it can be observed in Fig. 9 (f) and (h), that in both humid EA-treated PP/TiO_2 and PP/MgO samples, surface functionalization reduces charge injection and lowers the peak of homocharges. Grafted surface functionalization resulted in a lower water amount, as reported in [7], which leads to less water ionization ions and thereby decreased charge accumulation compared to untreated samples. Among the functionalizations, the amino functional group of MA and EA in TiO_2 and MgO shows a clear lower charge accumulation than the methacrylate of MM. The difference in electronegativity between amino and methacrylate would result in varied bonding states with water molecules, thereby leading to different capabilities in capturing charge carriers.

E. Electric Field Distortion

The field enhancement factor (FEF) was calculated based on the equation in [25]. Table II shows the FEF_D and FEF_H, or field enhancement factor of vacuum-dried and humid samples, of PP/TiO_2 and PP/MgO nanocomposites. The variation of field enhancement $FEF_{(H-D)}$ of neat PP did not differ between the humid and vacuum-dried samples. Humid nanocomposites, on the other hand, had greater FEF_H in comparison to their vacuum-dried samples, which is caused by increased charge accumulation in the materials. In humid untreated PP/TiO_2, the $FEF_{(H-D)}$ increases by 17.5%, while treated samples exhibited increases of 5-12.5%. In comparison to PP/TiO_2 samples, the enhanced FEF_H in humid PP/MgO samples was lower. The increased $FEF_{(H-D)}$ of humid untreated MgO was 15.5%, while the increased $FEF_{(H-D)}$ in treated MgO was 2.5-7.5%. Therefore, in both untreated and treated PP/MgO samples, the value of $FEF_{(H-D)}$ is lower than in PP/TiO_2 samples under the same surface conditions. This can be attributed to a reduced increase in charge accumulation, even though PP/MgO samples exhibit higher water absorption.

V. DISCUSSION

A. Nanoparticle Types

At filler content of 5 wt.%, the untreated samples exhibit varying degrees of charge accumulation depending on the nanoparticle used. Specifically, the PP/MgO sample is more effective in suppressing space charge injection and DC conductivity compared to PP/TiO_2. Under vacuum-dried conditions, both 5 wt.% untreated PP/TiO_2 and PP/MgO samples show similar agglomeration, crystallinity, and crystal structures. This suggests that changes in the microstructure at this high filler content do not directly link to the space charge dynamics and DC conductivity.

When considering electronic properties, i.e., band gap, it has been reported that TiO_2 possesses a band gap of 3.2 eV [26], while MgO has a band gap of 7.8 eV [27], and PP exhibits a band gap of 8.4 eV [28]. The systems discussed in this work are in line with the model proposed by Kubyshkina *et al.* [9][10], where they used DFT to study the behavior of zinc oxide (ZnO) in PE and PE/MgO samples. The authors suggested that systems with nanoparticles have significantly narrower band gaps than the polymer matrix, i.e., PE/ZnO samples exhibit the lowest energy state within the whole particle, thereby acting as charge carrier traps. Another mechanism as described in [9], involves using the high band gap of MgO in PE, which causes band bending at the interfaces, leading to the localization of the lowest energy states.

Compared to the results obtained from untreated PP/TiO_2 and PP/MgO samples, the use of nanoparticles with significantly narrower band gaps than the PP matrix, particularly TiO_2, promotes increased charge injection. These injected charges can be transported in the bulk of 5 wt.% materials as a result of the agglomeration. Conversely, band bending occurs at the interfaces in PP/MgO, otherwise; charge accumulation would be higher than in PP/TiO_2 due to the compatible band gaps between PP and MgO. This band bending is highly effective in capturing charge carriers and limiting their movement within the bulk materials. As a result, 5 wt.% untreated PP/MgO exhibits better charge suppression when compared to both neat PP and 5 wt.% untreated PP/TiO_2.

B. Surface Functionalization

While 5 wt.% treated nanoparticles tend to agglomerate, resulting in a poor dispersion within the PP matrix, the use of surface functionalization leads to decreased charge injection in PP/TiO_2 and PP/MgO samples under vacuum-dried conditions. Surface-modified TiO_2 and MgO nanofiller have methacrylate and amino organofunctional groups, which contain –O– and –N– moieties, respectively. These functional groups are exposed to the PP matrix and have chemical properties that differ from those of a hydrocarbon (–C– and –H–). The introduction of polar molecules with high electronegativity can alter the electronic structure at the interface, thereby potentially acting as traps within the interfaces, and affecting charge carrier movement along the nanoparticle surface [6]. The results in [9][29] demonstrate that the silicon-based functionalization of MgO-grafted nanoparticles effectively eliminates hydroxyl

TABLE II
THE FEF OF VACUUM-DRIED AND HUMID CONDITIONS IN 5 WT.% PP/TiO_2 AND PP/MgO NANOCOMPOSITES.

Samples	Field Enhancement Factor (%)		Variation (%)
	$FEF_{(D)}$	$FEF_{(H)}$	$FEF_{(H-D)}$
Neat PP	7.5	7.5	–
PP/TiO_2/5	17.5	35	17.5
PP/TiO_2/MM/5	7.5	20	12.5
PP/TiO_2/MA/5	7.5	15	7.5
PP/TiO_2/EA/5	7.5	12.5	5
PP/MgO/5	7	22.5	15.5
PP/MgO/MM/5	5	12.5	7.5
PP/MgO/MA/5	5	10	5
PP/MgO/EA/5	5	7.5	2.5

groups on nanoparticle surfaces. Consequently, this functionalization leads to a 1.7 eV wider band gap compared to the system without any functionalization.

C. Humidity

Besides the effects of humidity on degradation of dielectric properties in polymer nanocomposites, which have been widely reported [30][31], humidity can be used to investigate the impacts of using different surface functionalization and nanoparticles in determining dielectric properties in polymer matrix. The results in [7] show that when exposed to humid conditions, nanocomposites of 5 wt.% PP/TiO_2 and PP/MgO with different SCA exhibited distinct polarizability, which was influenced by the bonding state of water and polar functionalization. In simpler terms, the variations in measured relaxation peaks are attributed to the surface SCA types rather than the bulk properties of the nanoparticles.

Regarding charge transport, the dominant formation is homocharge. Heterocharge resulting from the ionization of water to form H_3O^+ and OH^- ions, is not readily observed, due to the significantly lower number of water ions compared to the total charges present in the bulk materials. The presence of water molecules, which leads to higher electrical conductivity and increased charge injection compared to the vacuum-dried samples, suggests that absorbed moisture can reduce the energy barrier between the samples and the electrodes [32]. This, along with the assumption of conductive pathway formation at the interfaces between the polymer and nanoparticles [33], facilitates the easier movement of charge carriers in humid samples [32][34]. The higher charge injection immediately within the bulk materials after applying a DC voltage may, in turn, result in a reduction in the measured charge density of heterocharge from water ionization, as the PEA technique can only measure net charges in the samples.

When comparing untreated samples, it was observed that PP/TiO_2 was characterized by approximately 0.45% less water absorption compared to PP/MgO. Upon calculating the amount of H_3O^+ and OH^- ions from water uptake, the amounts of each water ion components per unit volume are 2.1×10^{10} m^{-3} for untreated PP/MgO and 7.6×10^{9} m^{-3} for untreated PP/TiO_2. More water ions in untreated PP/MgO would result in more charge accumulation than untreated PP/TiO_2. However, the charge increase observed in humid PP/MgO samples was lower compared to its vacuum-dried sample, in contrast to humid PP/TiO_2. This indicates that the amount of water absorbed is not the only determinant of charge accumulation. Instead, variations in charge dynamics can also be influenced by the electronic properties, such as band gaps, of both water and nanoparticles. The presence of water molecules, which have a band gap of 6.9 eV [35], interacting with the nanoparticle surfaces, leads to changes in the lowest energy states, as described by Kubyshkina's model [9][10]. In the case of PP/MgO, band bending at the interface has the potential to counteract the increase in charge accumulation, even though the material absorbs more water.

For different surface functionalization, the more polar MM results in agglomeration 1-2 μm larger compared to MA and EA samples [7]. However, in terms of water absorption, it was found that MM-treated samples exhibited no significant difference in water absorption compared to MA-treated samples in both PP/TiO_2 and PP/MgO [7]. The significantly lower charge accumulation observed in the MA samples suggests that neither the morphology nor the amount of water could be contributing factors to this charge suppression. It is possible, once again, that the bonding of water molecules and polar functionalization would be more significant in lowering charge accumulation in MA. The difference in electronegativity between the amino group of MA and the methacrylate group of MM would lead to distinct bonding states with water molecules. Consequently, this difference in bonding states results in varying energy band levels at the interfaces, which, in turn, leads to differences in their abilities to capture charge carriers.

In addition, the EA-amino functional group, which shares the same amino functional group as MA but has longer alkoxy hydrolyzable groups, exhibited the lowest charge accumulation. The lower amount of EA grafted onto the surface, as compared to MA in both PP/TiO_2 and PP/MgO, resulted in reduced water absorption. This, in turn, led to more effective charge suppression and reduced electrical conductivity.

VI. Conclusion

This study presents experimental results on the charge transport behavior of PP systems containing different nanoparticles with different surface functionalization. The behavior of charge accumulation and conductivity under vacuum-dried conditions is significantly influenced by the types of nanoparticles. It is assumed that band bending is occurring at the interfaces between PP and MgO, which effectively suppresses charge accumulation and decreases electrical conductivity compared to PP/TiO_2 nanocomposites.

When considering the different surface functionalizations used for both nanoparticles, we only observe a reduction of charge accumulation and conductivity. This reduction can be attributed to the introduction of polar SCA with differing electronegativity values, modifying the electronic structure at the interface. This has the potential to generate traps within the interfaces, thereby, affecting charge carrier movement.

It is proposed that the quantity of water absorbed is not the primary factor in determining the amount of space charge that forms or the electrical conductivity. Instead, such factors depend on the interactions between water molecules and nanoparticle surfaces. Although PP/MgO exhibits higher water absorption, the band bending at the interfaces counteracts the increase in charge accumulation. Also, the differences in electronegativity of surface functionalization would cause different bonding states with water molecules, resulting in varying energy band levels at interfaces. This significantly influences charge carrier movement in the materials.

Overall, the results emphasize the distinct charge mechanisms in PP with two different nanoparticle band gaps, highlighting the significant charge suppression observed in the PP/MgO sample due to band bending at interfaces. Additionally, the use of ethoxy-modified materials with amino

functional groups in the presence of water molecules can effectively suppress charge accumulation and decrease electrical conductivity. Therefore, the appropriate choice of nanoparticles and surface functionalization can determine the dielectric properties of polymer nanocomposites.

REFERENCES

[1] Y. Zhou *et al.*, "Polypropylene-based ternary nanocomposites for recyclable high-voltage direct-current cable insulation," *Compos. Sci. Technol. J.*, vol. 165, pp. 168–174, 2018.

[2] K. Lindqvist, M. Andersson, A. Boss, and H. Oxfall, "Thermal and mechanical properties of blends containing PP and recycled XLPE cable waste," *J. Polym. Environ.*, vol. 27, no. 2, pp. 386–394, 2019.

[3] A. Patti and D. Acierno, "Thermal Conductivity of Polypropylene-Based Materials," in *IntechOpen*, 2019.

[4] J. Gao, H. Liu, T. Lee, U. Schachtely, H. Kobayashi, and L. Li, "Effect of hydrophilic/hydrophobic nanostructured TiO2 on space charge and breakdown properties of polypropylene," *Polymers (Basel).*, vol. 14, no. 14, p. 2762, 2022.

[5] G. Zhang *et al.*, "Space charge characteristics and breakdown properties of nanostructured SiO2/PP composites," *Polymers (Basel).*, vol. 15, no. 3, p. 2826, 2023.

[6] X. He *et al.*, "Silica surface-modification for tailoring the charge trapping properties of PP/POE based dielectric nanocomposites for HVDC cable application," *IEEE Access*, vol. 8, pp. 87719–87734, 2020.

[7] P. Ketsamee, T. Andritsch, and A. Vaughan, "The effects of humidity on dielectric permittivity of surface-modified TiO2- and MgO-based polypropylene nanocomposites," *IEEE Trans. Dielectr. Electr. Insul.*, vol. 30, no. 1, pp. 82–89, 2023.

[8] P. Ketsamee, T. Andritsch, and A. Vaughan, "Effect of surface-modified TiO2 and MgO nanoparticles on dielectric permittivity and breakdown strength of PP nanocomposites," in *IEEE Conference on Electrical Insulation and Dielectric Phenomena*, 2021, pp. 1–4.

[9] E. Kubyshkina, M. Unge, and B. L. G. Jonsson, "Communication: Band bending at the interface in polyethylene-MgO nanocomposite dielectric," *J. Chem. Phys.*, vol. 146, p. 051101, 2017.

[10] E. Kubyshkina, B. L. G. Jonsson, and M. Unge, "ZnO-polyethylene interface : Band alignment," in *International Symposium on Electrical Insulating Materials (ISEIM)*, 2017, pp. 363–365.

[11] X. Wang, T. Andritsch, and G. Chen, "Influence of the amount of silane coupling agent on the dielectric properties of AlN/polypropylene nanocomposites," in *IEEE Conference on Electrical Insulation and Dielectric Phenomena*, 2019, pp. 356–359.

[12] F. A. CAREY and R. J. SUNDBERG, *Advanced Organic Chemistry Part A: Structure and Mechanisms*, Fifth Edit. VA, USA: Springer, 2007.

[13] S. M. Davachi, B. S. Heidari, R. Sahraeian, and A. Abbaspourrad, "The effect of nanoperlite and its silane treatment on the crystallinity, rheological, optical, and surface properties of polypropylene/nanoperlite nanocomposite films," *Compos. Part B Eng.*, vol. 175, p. 107088, 2019.

[14] T. Theivasanthi and M. Alagar, "Titanium dioxide (TiO2) nanoparticles XRD analyses: An insight," *Chem. Phys.*, 2013.

[15] C. Kagenda *et al.*, "Silicone elastomer composites fabricated with MgO and MgO-multi-wall carbon nanotubes with improved thermal conductivity," *Nanomaterials*, vol. 11, no. 12, p. 3418, 2021.

[16] E. B. Bond, J. E. Spruiell, and J. S. Lin, "A WAXD/SAXS/DSC study on the melting behavior of Ziegler–Natta and metallocene catalyzed isotactic polypropylene," *J. Polym. Sci. Part B Polym. Phys.*, vol. 37, no. 21, pp. 3050–3064, 1999.

[17] E. Tarani, I. Arvanitidis, D. Christofilos, D. N. Bikiaris, K. Chrissafis, and G. Vourlias, "Calculation of the degree of crystallinity of HDPE/GNPs nanocomposites by using various experimental techniques: A comparative study," *J. Mater. Sci.*, vol. 58, no. 4, pp. 1621–1639, 2023.

[18] K. Al Imran, J. Lou, and K. N. Shivakumar, "Enhancement of electrical and thermal conductivity of polypropylene by graphene nanoplatelets," *J. Appl. Polym. Sci.*, vol. 135, no. 9, p. 45833, 2018.

[19] L. K. H. Pallon *et al.*, "The impact of MgO nanoparticle interface in ultra-insulating polyethylene nanocomposites for high voltage DC cables," *J. Mater. Chem. A*, vol. 4, no. 22, pp. 8590–8601, 2016.

[20] N. A. M. Jamail, M. A. M. Piah, N. A. Muhamad, R. A. Zainir, N. F. Bin Kasri, and Q. E. Kamarudin, "DC conductivity of polymer nanocomposites for different types and amount of nanofiller," *Int. J. Electr. Eng. Informatics*, vol. 5, no. 2, pp. 217–225, 2013.

[21] R. Ayoob, "Dielectric properties of hexagonal boron nitride polymer nanocomposites," University of Southampton, Southampton, UK, 2017.

[22] N. Liu, C. Zhou, G. Chen, and L. Zhong, "Determination of threshold electric field for charge injection in polymeric materials," *Appl. Phys. Lett.*, vol. 106, no. 19, p. 192901, 2015.

[23] F. Zheng, G. Teyssedre, C. Laurent, Ć. Thomas, M. Hoyos, and Y. Zhang, "Charge injection and charge separation as revealed by dynamic space charge measurement in poly(propylene-ethylene) copolymer films," *J. Appl. Phys.*, vol. 104, p. 094104, 2008.

[24] L. Hui, L. Schadler, and J. Keith Nelson, "The influence of moisture on the electrical properties of crosslinked polyethylene/silica nanocomposites," *IEEE Trans. Dielectr. Electr. Insul.*, vol. 20, no. 2, pp. 641–653, 2013.

[25] P. Morshuis and M. Jeroense, "Space charge measurements on impregnated paper: A review of the PEA method and a discussion of results," *IEEE Electr. Insul. Mag.*, vol. 3, no. 3, pp. 26–35, 1997.

[26] C. Dette *et al.*, "TiO2 anatase with a bandgap in the visible region," *Nano Lett.*, vol. 14, no. 11, pp. 6533–6538, 2014.

[27] U. Schönberger and F. Aryasetiawan, "Bulk and surface electronic structures of MgO," *Phys. Rev. B*, vol. 52, no. 12, pp. 8788–8793, 1995.

[28] H. Xie, X. Wu, Z. Peng, and H. Zhang, "The energy criterion for breaking chemical bonds in electrical breakdown process of polymer," in *Proceedings of the IEEE International Conference on Properties and Applications of Dielectric Materials*, 1994, pp. 39–41.

[29] E. Kubyshkina, B. L. G. Jonsson, and M. Unge, "Ab-initio modeling of interfacial region in nanocomposite dielectrics," in *2015 Electrical Insulation Conference (EIC)*, 2015, pp. 618–620.

[30] D. Qiang, Y. Wang, X. Wang, G. Chen, and T. Andritsch, "The effect of filler loading ratios and moisture on DC conductivity and space charge behaviour of SiO2 and hBN filled epoxy nanocomposites," *J. Phys. D. Appl. Phys.*, vol. 52, no. 39, p. 395502, 2019.

[31] J. Yang, X. Wang, H. Zhao, W. Zhang, and M. Xu, "Influence of moisture absorption on the DC conduction and space charge property of MgO/LDPE nanocomposite," *IEEE Trans. Dielectr. Electr. Insul.*, vol. 21, no. 4, pp. 1957–1964, 2014.

[32] M. Praeger, I. L. Hosier, A. F. Holt, A. S. Vaughan, and S. G. Swingler, "On the effect of functionalizer chain length and water content in polyethylene/silica nanocomposites: Part II – charge transport," *IEEE Trans. Dielectr. Electr. Insul.*, vol. 24, no. 4, pp. 2410–2420, 2017.

[33] C. Zou, J. C. Fothergill, and S. W. Rowe, "The effect of water absorption on the dielectric properties of epoxy nanocomposite," *IEEE Trans. Dielectr. Electr. Insul.*, vol. 15, no. 1, pp. 106–117, 2008.

[34] Y. Wang, D. Qiang, F. N. F. Alhabill, Z. Xu, G. Chen, and A. Vaughan, "Influence of moisture absorption on electrical properties and charge dynamics of polyethylene silica-based nanocomposites," *J. Phys. D. Appl. Phys.*, vol. 51, p. 425302, 2018.

[35] A. Shimkevich, "Electrochemical view of the band gap of liquid water for any solution," *World J. Condens. Matter Phys.*, vol. 4, pp. 243–249, 2014.